Available online at BCREC website: https://bcrec.id

Bulletin of Chemical Reaction Engineering & Catalysis, 14 (3) 2019, 625-633

Research Article

# Tuning the Morphology of $Ag_3PO_4$ Photocatalysts with an Elevated Concentration of $KH_2PO_4$

**Khusnul Afifah, Roy Andreas, Dadan Hermawan, Uyi Sulaeman***

*Department of Chemistry, Jenderal Soedirman University, Purwokerto, 53123, Indonesia*

*Received: 6th April 2019; Revised: 8th August 2019; Accepted: 8th August 2019; Available online: 30th September 2019; Published regularly: December 2019*

**Abstract**

Tuning the morphology of $Ag_3PO_4$ photocatalysts with an elevated concentration of $KH_2PO_4$ have been successfully conducted. This photocatalyst was prepared by starting material of $AgNO_3$ and $KH_2PO_4$. The $KH_2PO_4$ aqueous solution with five concentrations of 0.10 M, 0.15 M, 0.30 M, 0.45 M, and 0.60 M was reacted with $AgNO_3$ aqueous solution. The products were characterized using X-ray Diffraction (XRD), UV-Vis Diffuse Reflectance Spectroscopy (DRS), and Scanning Electron Microscopy (SEM). The concentration of $KH_2PO_4$ significantly affected the morphology, size, and crystallinity of catalyst. The morphology of $Ag_3PO_4$ may be tuned with the synthesis using an elevated concentration of $KH_2PO_4$. The sample with the synthesis using 0.15 M of $KH_2PO_4$ exhibited the excellent photocatalytic activity. The high photocatalytic activity was caused by the small size of mixed morphology of sphere and tetrahedron, high crystallinity and defect sites. 

***Keywords***: photocatalyst; $Ag_3PO_4$; tetrahedron; $KH_2PO_4$; defect sites

***How to Cite***: Afifah, K., Andreas, R., Hermawan, D., Sulaeman, U. (2019). Tuning the Morphology of $Ag_3PO_4$ Photocatalysts with an Elevated Concentration of $KH_2PO_4$. *Bulletin of Chemical Reaction Engineering & Catalysis*, 14(3): 625-633 (doi:10.9767/bcrec.14.3.4649.625-633)

***Permalink/DOI***: https://doi.org/10.9767/bcrec.14.3.4649.625-633

## 1. Introduction

Environmental pollution caused by the disposal of textile industry liquid waste has become a serious problem. It may provide a negative impact on humans, animals and aquatic ecosystems because the textile dye waste is highly toxic [1]. These problems have taken the attention of many researchers in the world to find a solution by developing and discovering the effective and environmentally friendly textile wastewater treatment technology. The photocatalysis, a chemical reaction under photon light, may become one effective method when applied for textile wastewater treatment.

A new candidate of photocatalyst, silver orthophosphate ($Ag_3PO_4$), exhibits an effective and efficient photocatalyst due to a very high oxidation activity under visible light irradiation [2]. It is proven that the $Ag_3PO_4$ has excellent photocatalytic activity with a quantum yield of 90% and has a band gap energy of 2.43 eV. The $Ag_3PO_4$ photocatalyst is very potential to degrade the organic compound of Rhodamine B [3], bisphenol A [4,5], phenol [6,7], methylene blue [8], microcystins [9], and atrazine herbicide [10].

$Ag_3PO_4$ photocatalysts may be synthesized by several methods. Coprecipitation [5,11], hydrothermal [8], sonochemical [12,13], and ultrasound-assisted synthesis [14] have been used to prepare this photocatalyst. Many researchers have designed the $Ag_3PO_4$-based composites to enhance the catalytic activity. The composite of

* Corresponding Author.
E-mail: uyi_sulaeman@yahoo.com (U. Sulaeman);
Telp: +62-281-638793, Fax: +62-281-638793

$Ag_3PO_4$/g-$C_3N_4$ [15], $Ag_3PO_4$/$MoS_2$ [16], and $Ag_3PO_4$-coated carbon microspheres [17] may be designed with the hydrothermal synthesis. Graphene/$Ag_3PO_4$ quantum dots [12] and $Ag_3PO_4$ nanospheres [18] may be prepared using a sonochemical process. The composites of $Ag_3PO_4$/g-$C_3N_4$ [19], $Ag_3PO_4$/$Ag_2W_2O_7$ heterojunction [20], and $Ag_3PO_4$-graphene [21] may be synthesized using co-precipitation method. Beside the composites design, the key point of the enhanced $Ag_3PO_4$ photocatalyst is due to the morphological modification which may be conducted using the precipitation, ion exchange and hydrothermal method [22]. Finding the simple method in controlling the morphology is very important to apply in large-scale synthesis. Modifying the starting materials, *e.g.* type of starting material and concentration may be conducted to gain the morphology which has a high catalytic activity.

The researchers have used the starting material of $Na_2HPO_4$ as a source of phosphate ion [23,24,25]. The starting material of phosphate ion source is very important because it may change the morphology and size. Phosphoric acid ($H_3PO_4$) may be used to produce the morphology of tetrahedron [26]. Adding the oleic acid to this preparation leads to the formation of homogeneous tetrahedral morphology. The hydroxyapatite synthesized from $KH_2PO_4$ and $CaCl_2$ may be used as a starting material to form a sphere of highly active $Ag_3PO_4$ catalyst [27]. Recently, the $KH_2PO_4$ may also be used directly as a source of phosphate ion in the co-precipitation method [28]. It is very impressive that the concentration of $KH_2PO_4$ may affect the morphology of $Ag_3PO_4$. However, this report has not investigated the tuning morphology to obtain the highest photocatalytic activity. Therefore, the aim of this research is to figure out the optimum photocatalytic activity of $Ag_3PO_4$ using the elevated concentration of $KH_2PO_4$ as a source of phosphate ion.

## 2. Materials and Methods

### 2.1 Synthesis of $Ag_3PO_4$

The synthesis of $Ag_3PO_4$ was conducted based on Dong's method [28] with modification. The starting material of $AgNO_3$ (Merck) and $KH_2PO_4$ (Merck) were used in this preparation. The concentration of 0.1 M $AgNO_3$ aqueous solution was designed by dissolving 1 gram in 50 mL of solution. The $KH_2PO_4$ aqueous solution, with five concentrations of 0.10 M, 0.15 M, 0.30 M, 0.45 M, and 0.60 M, were prepared. These solutions were used for samples of K-10, K-15, K-30, K-45, and K-60, respectively. The 50 mL of $AgNO_3$ solution was mixed with 20 mL of $KH_2PO_4$ solution drop by drop under stirring up to 2 hours until the yellow precipitates formed. The mixture was then filtered and washed with deionized water several times. The products were dried at 105 °C in the oven for 30 minutes.

### 2.2 Characterization of $Ag_3PO_4$

The crystal structure of $Ag_3PO_4$ was determined using the XRD (Shimadzu 7000). The absorption and band gap energy were determined using UV-VIS DRS (JASCO V-670). To investigate the morphology, the samples were characterized using SEM (JEOL JSM-6510LA).

### 2.3 Photocatalytic Activity Evaluation

The photocatalyst of 0.1 g was put into 100 ml of Rhodamine B solution 10 ppm in a beaker glass, and placed on a plate stirrer and then stirred using a magnetic stirrer in dark conditions for 20 minutes [27]. This suspension was then irradiated with a blue LED light (OptiLED, 2.5 W, $\lambda$ = 455 nm) for 40 minutes. Samples (5 mL) were taken periodically every 10 minutes and put into a centrifuge tube. The suspension was centrifuged at a speed of 2000 rpm for 30 minutes to separate the photocatalyst from the solution. The absorbance of the solution was measured using a spectrophotometer (Shimadzu 1800 UV-Vis). The highest activity of photodegradation was also monitored using the HPLC (Hitachi) equipped with a Brownie Choice C18 column (150 mm × 4.6 mm, 5 μm), UV-VIS Detector L-2420 and Autosampler L-2200. Mobil phase of HPLC was a mixture of acetonitrile: water (75:25, v/v) at a flow rate of 1 mL $min^{-1}$ and the volume injection of sample is 20 μL. The detection of RhB was conducted at wavelength of 554 nm.

### 2.4 Reusability of Photocatalyst

The reusability of photocatalyst was evaluated using RhB degradation up to 4 times recycling the catalytic activity [27]. The highest activity of photocatalyst $Ag_3PO_4$ as much as 0.1 gram was put into 100 mL of Rhodamine B solution 10 ppm. A blue LED was turned on after a 20 minutes dark reaction. Every 10 minutes, 5 mL samples were taken from the solution. The samples were then centrifuged at a speed of 2000 rpm for 30 minutes. The concentration of RhB was measured by UV-vis spectrophotometer. The precipitate was collected, washed with deionized water and dried at 105 °C for 30

minutes. The obtained precipitates were tested again for their degradation activity.

## 3. Results and Discussion

### 3.1 Synthesis of Photocatalyst

The synthesis of $Ag_3PO_4$ photocatalyst was conducted by mixing the starting material of $AgNO_3$ and $KH_2PO_4$ at the elevated concentration from 0.10 M to 0.60 M. Yellow precipitates were successfully formed from the mixture solution. The reaction of co-precipitation is written as follows (Equation (1)):

$$3AgNO_{3(l)} + 3KH_2PO_{4(l)} \rightarrow Ag_3PO_{4(s)} + 3KNO_{3(l)} + 2H_3PO_{4(l)} \quad (1)$$

The byproduct of potassium nitrate and phosphoric acid can be dissolved in water and easy to remove from the $Ag_3PO_4$ through washing. The variation of concentration produces the same color as precipitates.

### 3.2 Photocatalyst Characterization

To determine the structure and crystallinity, the three products with a different concentration of 0.10 M, 0.15 M, and 0.60 M, namely K-10, K-15, and K-60, respectively, were characterized using XRD. The results may be seen in Figure 1(a). The peaks observed in diffractogram are fit with the standard data (JCPDS 06-0505) which have a structure of body-centered cubic [29,30]. There are no other peaks observed in the diffractogram, meaning that the samples are pure. The value of 2 theta is shifted by increasing the concentration, indicating that the elevated concentration of $KH_2PO_4$ may change the lattice constant of crystal (Figure 1(b)). These changes may be induced by changing morphology from sphere to tetrahedron. During the changing of morphology some unique structures of K-15 may be observed. The high intensity of diffractogram of K-15 was observed, indicating that the sample had higher crystallinity. It is possible that the high crystallinity may form the defect in the crystal that generates the broad absorption both in UV and the visible region as shown in Figure 2.

The three-sample spectra absorptions were observed using the DRS from 380 nm to 780 nm. The results are shown in Figure 2. The absorption spectra of K-15 were higher than that of K-10. However, the K-60 exhibited the lowest absorption. It indicated that the concentration of $KH_2PO_4$ may not linearly increase the absorption spectra. The higher absorption may be observed in K-15 that it may be related to the high crystallinity and defect formation. Some researchers have reported that the defect may change the absorption of visible wavelength [31] and lattice constant [32]. It is greatly useful that the defect may be generated by changing the concentration of starting material. There is no need to use much energy, such as calcination treatment. Therefore, it is highly beneficial for the commercial application.

Band gaps are the representative of effective wavelength absorbed in which the electrons may be exited. The band gap of a photocatalyst may be determined using the Tauc formula which correlates the absorption of photon energy [33]. The Tauc formula is shown as follows: (2)

$$\alpha h\nu = A\left(h\nu - E_g\right)^{n/2} \quad (2)$$

where $E_g$, $\alpha$, and $A$ are band gap energy, ab-

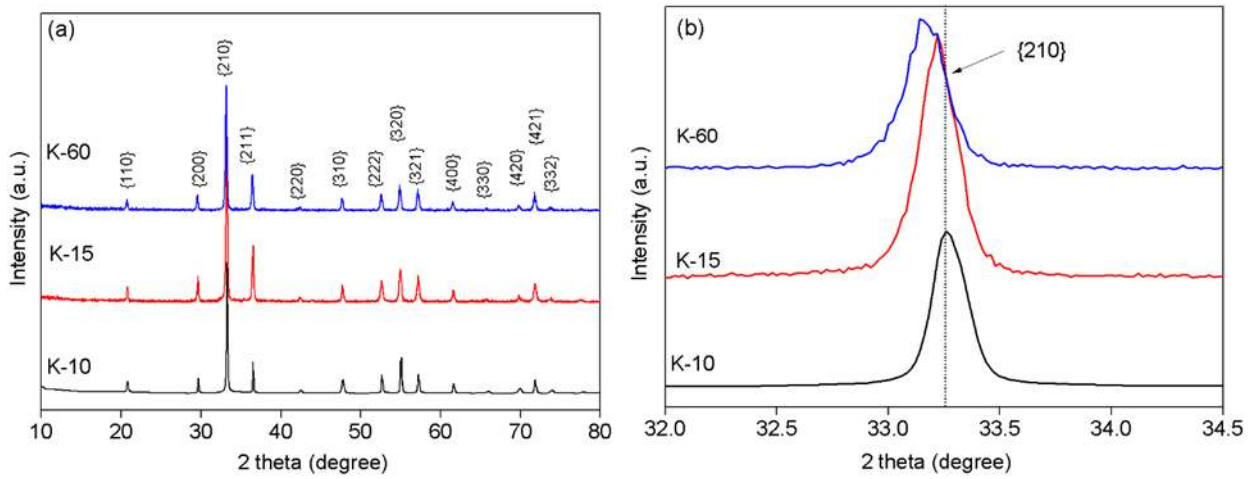


**Figure 1**. The XRD pattern of $Ag_3PO_4$ synthesized with different concentration of $KH_2PO_4$ (a) and the shift of 2 theta at {210} (b).

sorption coefficient, and constant, respectively. The value of $n$ depends on type transition, the indirect semiconductor ($n$ = 4) or direct transition state ($n$ = 1). Based on the plot $(\alpha hv)^2$ as a function of $hv$, the band gap energy of a photocatalyst can be measured by extrapolating the linear absorption point on the curve which intersects the x-axis of energy ($hv$) [34]. Band gap energies of 2.38 eV, 2.39 eV and 2.33 eV were obtained from the sample of K-10, K-15 and K-60, respectively (Figure 2 (b, c, d)). The $E_g$ of K-10 and K-15 was relatively similar, indicating that this different catalytic activity was not caused by the energy gap. The sample of K-60 had lower band gap energy which decreased up to 0.05 when compared with K-10 and decreased up to 0.04 when compared with K-15.

The morphology of the particles from the photocatalyst of K-10, K-15, and K-60, were investigated by SEM. The results may be seen in Figure 3. The mixed morphologies of sphere and cube with 2-3 μm in diameter were observed in the sample of K-10. These morphologies were changed into the mixed of sphere and tetrahedron after increasing the concentration of $KH_2PO_4$ as found in the sample of K-15. This particle size is relatively similar to K-10. The unique tetrahedron with round corner can be clearly observed in K-15. This may be a transition of morphology changes from sphere to a tetrahedron. The large particle of the tetrahedron (5-8 μm) may be produced after increasing more $KH_2PO_4$ as shown in the sample of K-60 that the morphology is completely changed into a tetrahedron with a small amount of tripod shape.

The varied morphology of the sample indicated that the $KH_2PO_4$ concentration really affected the coprecipitation mechanism. The concentration differences may influence the nucleation and crystal growth. The morphology of catalyst material may be influenced and controlled by several factors, such as solvents, starting material, additives and synthesis methods [28,35].

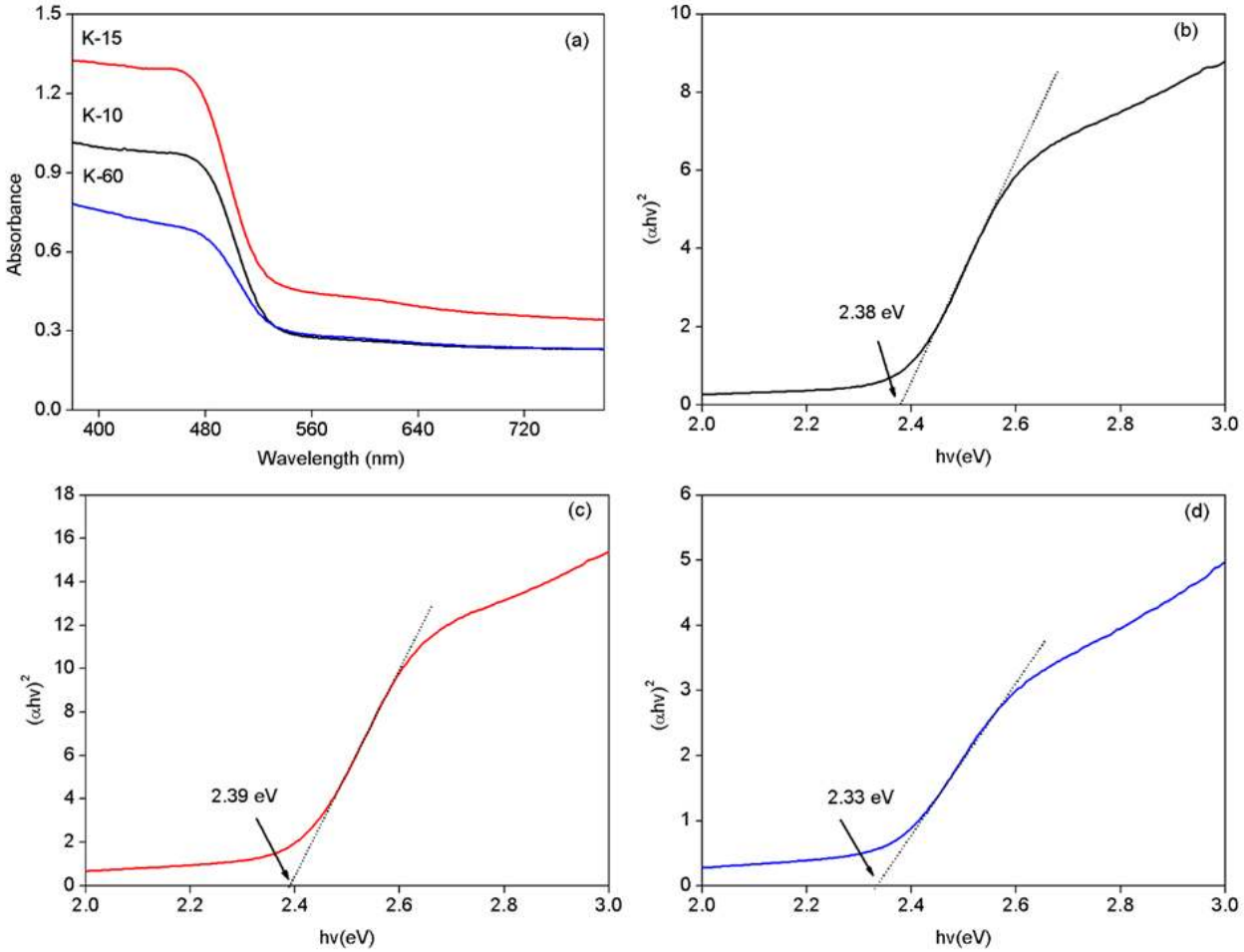


**Figure 2**. The DRS of $Ag_3PO_4$ synthesized with different concentration of $KH_2PO_4$ (a) and their calculation of band gap energy of the sample K-10 (b), K-15 (c) and K-60 (d).

3.3 Photocatalytic Activity Test

The photocatalytic activity tests of K-10, K-15, K-30, K-45 and K-60 samples were conducted through the RhB degradation under blue light irradiation. The decreased concentration of RhB was monitored under UV-VIS spectrophotometer. Figure 4 showed the profile of catalytic activity due to the different concentration of $KH_2PO_4$. The pseudo first order kinetic reaction was investigated using the equation (3) [36]:

$$\ln\left(\frac{C_0}{C_t}\right) = kt \quad (3)$$

where $k$, $C_0$, and $C_t$ are the first order pseudo rate constant, initial concentration and the concentration at a given reaction time, respectively [3]. The rate constant is calculated from the slope of linear regression. The rate constant of 0.081 $min^{-1}$, 0.132 $min^{-1}$, 0.052 $min^{-1}$, 0.038 $min^{-1}$, 0.017 $min^{-1}$ was found in K-10, K-15, K-30, K-45 and K-60, respectively. The

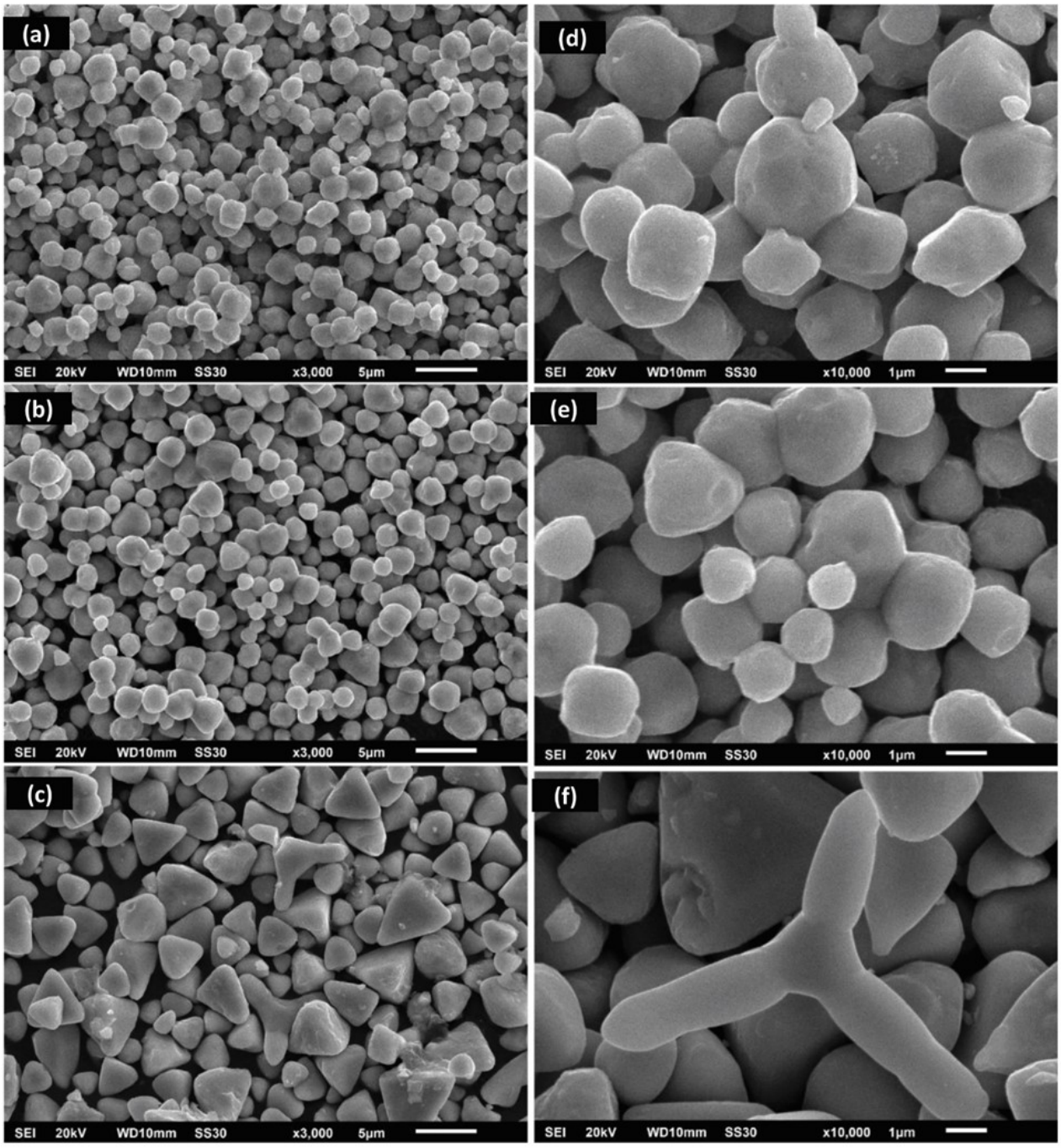


**Figure 3**. SEM images of K-10 (a), K-15 (b), and K-60 (c) with high magnification of K-10 (d), K-15, and K-60 (f).

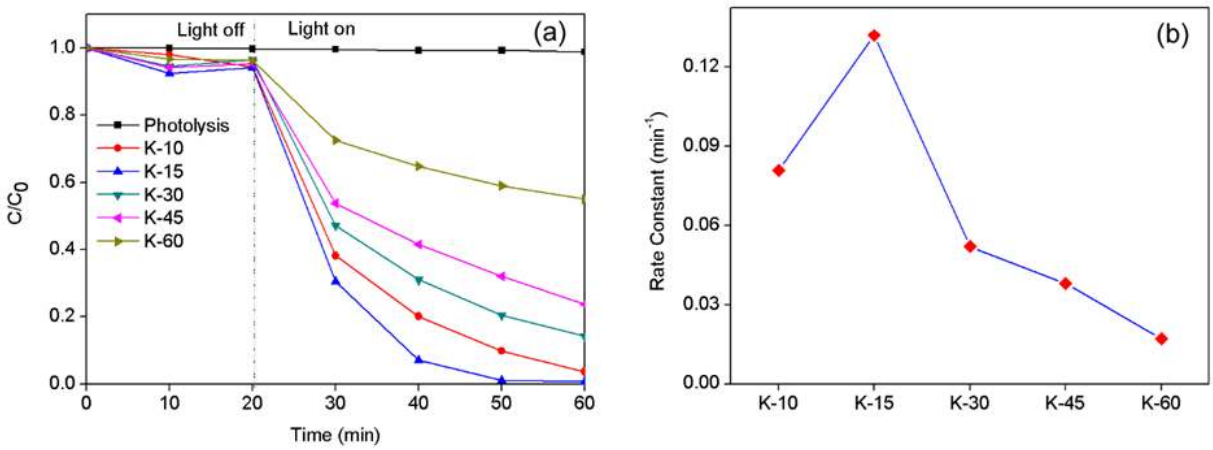


**Figure 4**. Photocatalytic activities of $Ag_3PO_4$ synthesized using a different concentration of $KH_2PO_4$ as a source of phosphate ion (a) and their rate constant (b).

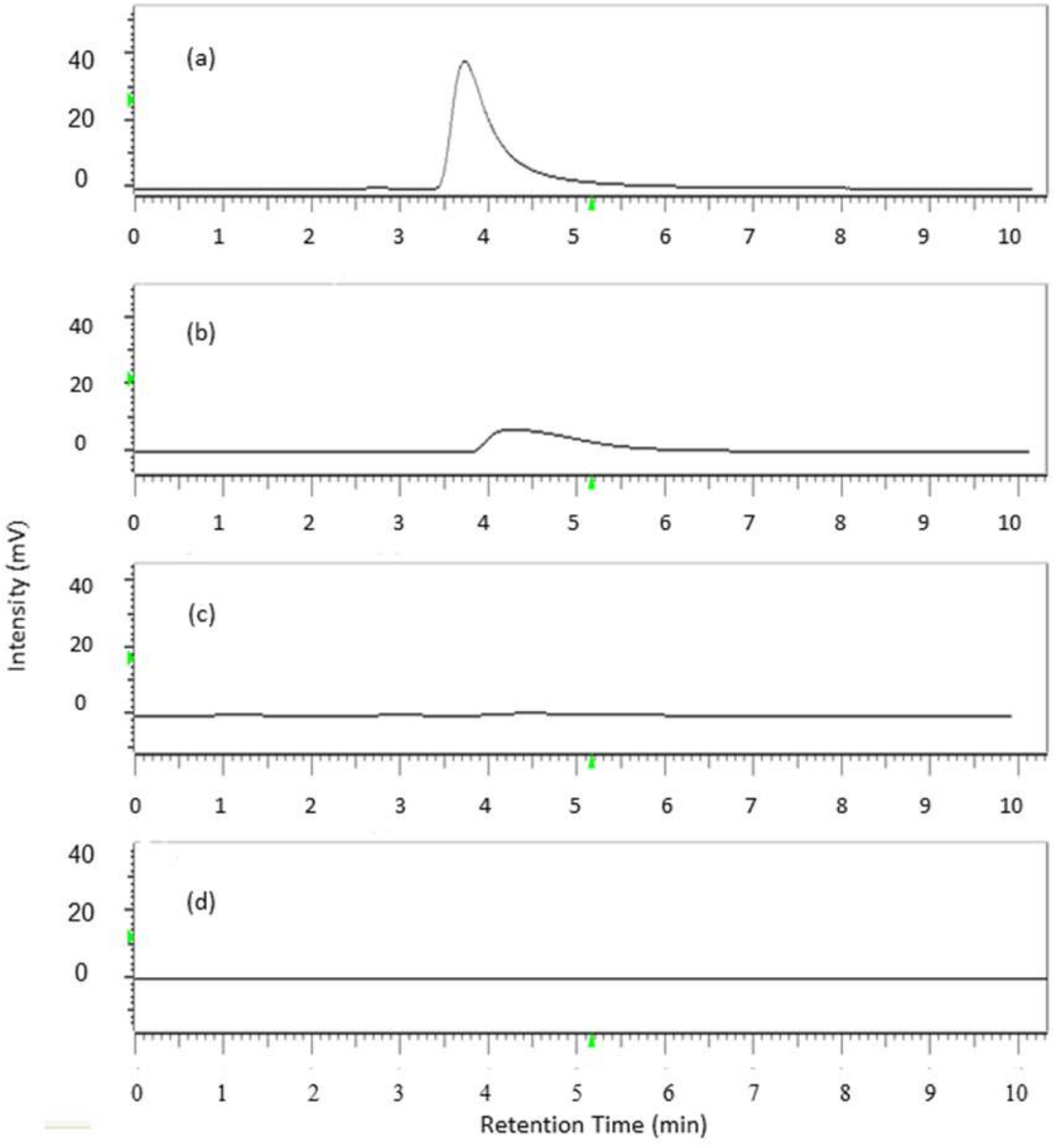


**Figure 5**. The degradation of RhB monitored using the HPLC, (a) initial concentration of RhB (10 mg/L), and after (b) 10 minutes, (c) 20 minutes, (d) 30 minutes of photodegradation.

highest catalytic activity may be found at a concentration of 0.15 M (K-15). When the concentration of $KH_2PO_4$ increases from 0.30 to 0.60 M, the catalytic activity gradually decreases. It indicates that the concentration of $KH_2PO_4$ may affect the properties of $Ag_3PO_4$. The highest photocatalytic activity was also investigated using the HPLC. The peak of RhB can be clearly detected at the retention time of 3.73 minutes (Figure 5). After 10 minutes of photocatalytic reaction, the RhB concentration decreased from 10 mg/L to 3.1 mg/L, and it completely degraded after 30 minutes reaction. These results are similar with those conducted with the UV-VIS spectrophotometer measurement as shown in Figure 4.

The changes of $Ag_3PO_4$ morphology are responsible in the surface catalytic reaction. The transition morphology from sphere to tetrahedron has improved the catalytic activity. Some researchers have reported that the tetrahedron morphology of $Ag_3PO_4$ had high surface energy [23] and high $Ag^+$ in the surface of {111} [37] which significantly contributed to high catalytic activity. In addition, the highly broad absorption of K-15 suggested that the defect might exist in the surface. High absorption implied that more photon may be used in the excitation of an electron from VB to CB. The lowest activity may be found in K-60. Thus, the sample of K-60 has a large particle with lower crystallinity and lower band gap energy. The large particle will have a small surface area which decreases the catalytic activity. The low crystallinity will inhibit the electron transfer in the surface of the catalyst. Too low band gap energy may increase the recombination of electron and hole pair. These all phenomena dramatically decrease the catalytic activity of $Ag_3PO_4$.

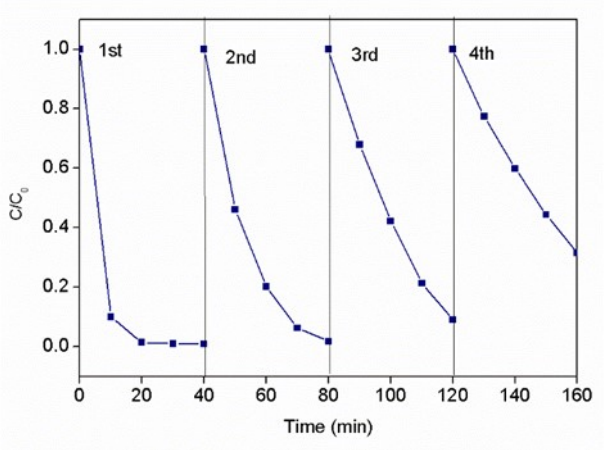


**Figure 6**. The reusability of photocatalyst of the highest catalytic activity (K-15).

Based on the spectrophotometer and HPLC measurement, the photocatalyst of $Ag_3PO_4$ completely degraded the organic compounds of Rhodamine B. This phenomenon was caused by the presence of electrons and holes formed due to the photon energy exposure. According to Liu *et al.* [29], when radiation is conducted, the electrons in the valence band (VB) may be exited to the conduction band (CB), generating the holes in VB. The holes species is a strong oxidizer which may oxidize the organic compound with an oxidation potential of +1.0 V to +3.5 V (relative to Hydrogen-Nernst electrodes).

There are several steps of RhB compound decomposition under $Ag_3PO_4$ photocatalysts. The first step is the breakdown of the $Cl^-$ group, the second step is the ethylated process of four ethyl groups ($C_2H_4$) which are bound to N atoms, the third step is deaminization of two amine groups ($NH_2$), the fourth step is decarboxylic ($COO^-$), the fifth and sixth steps are the breakdown of the chromophore ring and the breakdown of the aromatic ring that produces formic acid and acetic acid. The final products of this decomposition are water ($H_2O$) and carbon dioxide ($CO_2$) known as nontoxic compounds [38].

### 3.4 Reusability of Photocatalyst

To investigate the reusability of photocatalyst, the recycling photocatalytic activity of sample was conducted. The sample of highest catalytic activity was chosen to evaluate its reusability. The photocatalytic activities were repeated up to 4 cycles. The results may be seen in Figure 6. The ability of catalytic decreased gradually after the recycling test, indicating that the photocatalyst was relatively unstable. Many researchers have reported that the photo-corrosion is the main problem of low stability [39]. In this experiment, the color of photocatalyst changed into a dark solid due to the photo-corrosion that produces a metallic Ag adsorbed on the surface of $Ag_3PO_4$. It was the typical properties of unmodified $Ag_3PO_4$. The composite modification may prevent this phenomenon where the electron exited in $Ag_3PO_4$ may be used for further reaction instead of photo-corrosion.

## 4. Conclusion

The morphology of $Ag_3PO_4$ may be tuned with the synthesis using a varied concentration of $KH_2PO_4$. The sample with the synthesis using 0.15 M of $KH_2PO_4$ exhibited the excellent photocatalytic activity. The small size of mixed morphology of sphere and tetrahedron, high

crystallinity and formation of defect sites, have improved the catalytic activity. This result is the first stage to provide a highly active and stable $Ag_3PO_4$ photocatalyst. For the future research, this finding is very useful to design the $Ag_3PO_4$-based composite using tetrahedron morphology to prevent the instability of photocatalyst caused by the photo-corrosion.

## Acknowledgement

This research was financially supported by Directorate of Research and Community Services, Directorate General of Development and Research Enhancement, Ministry of Research, Technology and Higher Education of the Republic of Indonesia, 62/SP2H/LT/DRPM/2019, 2019.

## References

[1] Chen, K.C., Wua, J.Y., Huang, C.C. Liang, Y.M., Hwang, S.C.J. (2003). Decolorization of azo dye using PVA-immobilized microorganisms. *Journal of Biotechnology*, 101(3): 241−252.

[2] Yi, Z., Ye, J., Kikugawa, N., Kako, T., Ouyang, S., Stuart-Williams, H., Yang, H., Cao, J., Luo, W., Li, Z., Liu, Y., Withers, R.L. (2010). An orthophosphate semiconductor with photooxidation properties under visible-light irradiation. *Nature Materials,* 9: 559−564.

[3] Yan, X., Gao, Q., Qin, J., Yang, X., Li, Y., Tang, H. (2013). Morphology controlled synthesis of $Ag_3PO_4$ microcubes with enhanced visible light driven photocatalytic activity. *Ceramic International*, 39(8): 9715−9720.

[4] Katsumata, H.M., Taniguchi, S., Kaneco, S., Suzuki, T. (2013). Photocatalytic degradation of Bisphenol A by $Ag_3PO_4$ under visible light. *Catalysis Communications*, 34: 30−34.

[5] Li, T., Wei, H., Ji, H., Xi, T., Guo, X., Wang, T., Zhu, L. (2019). Mechanisms for highly efficient mineralization of bisphenol a by heterostructured $Ag_2WO_4/Ag_3PO_4$ under simulated solar light. *ACS Sustainable Chemistry & Engineering*, 7(4): 4177−4185.

[6] Fu, G., Xu, G., Chen, S., Lei, L., Zhang, M. (2013). $Ag_3PO_4/Bi_2WO_6$ hierarchical heterostructures with enhanced visible light photocatalytic activity for the degradation of phenol. *Catalysis Communications*, 40: 120−124.

[7] Song, S., Meng, A., Jiang, S., Cheng, B. (2018). Three-dimensional hollow graphene efficiently promotes electron transfer of $Ag_3PO_4$ for photocatalytically eliminating phenol. *Applied Surface Science*, 442: 224−231.

[8] Dhanabal, R., Chithambararaj, A., Velmathi, S., Bose, A.C. (2015). Visible light driven degradation of methylene blue dye using $Ag_3PO_4$. *Journal of Environmental Chemical Engineering*, 3(3): 1872−1881.

[9] Guo, Q., Li, H., Zhang, Q., Zhang, Y. (2018). Fabrication, characterization and mechanism of a novel Z-scheme $Ag_3PO_4$/NG/polyimide composite photocatalyst for microcystin-LR degradation. *Applied Catalysis B: Environmental*, 229: 192−203.

[10] Mohaghegh, N., Tasviri, M., Rahimi, E., Gholami, M.R. (2015). Comparative studies on $Ag_3PO_4/BiPO_4$–metal-organic framework–graphene-based nanocomposites for photocatalysis application. *Applied Surface Science*, 351: 216−224.

[11] Febiyanto, F., Soleh, A., Amal, M.S.K., Afif, M., Sewiji, S., Riapanitra, A., Sulaeman, U. (2019). Facile Synthesis of $Ag_3PO_4$ Photocatalyst with Varied Ammonia Concentration and Its Photocatalytic Activities For Dye Removal. *Bulletin of Chemical Reaction Engineering & Catalysis*, 14(1): 42-50.

[12] Reheman, A., Tursun, Y., Dilinuer, T., Halidan, M., Kadeer, K., Abulizi, A. (2018). Facile one-step sonochemical synthesis and photocatalytic properties of graphene/$Ag_3PO_4$ quantum dots composites. *Nanoscale Research Letters*, 13: 70.

[13] Zheng, C., Yang, H., Yang, Y., Zhang, H. (2018). Enhanced photocatalytic performance and mechanism of $Ag_3PO_4$ particles synthesized via a sonochemical process. *Nanoscience and Nanotechnology Letters*, 10(3): 337−345.

[14] Lin, W., Zhang, S., Wang, D., Zhang, C., Sun, D. (2015). Ultrasound-assisted synthesis of high-efficiency $Ag_3PO_4/CeO_2$ heterojunction photocatalyst. *Ceramics International*, 41(7): 8956−8963

[15] Zhao, Z., Fan, J., Liu, W., Xue, Y., Yin, S. (2017). In-situ hydrothermal synthesis of $Ag_3PO_4$/g-C3N4 composite and their photocatalytic decomposition of NOx. *Journal of Alloys and Compounds*, 695: 2812−2819.

[16] Saud, P.S., Pant, B., Ojha, G.P., Kim, D.U., Kuk, Y.S., Park, S.J., Park, M., Kim, H.Y. (2017). One-pot synthesis of $Ag_3PO_4/MoS_2$ nanocomposite with highly efficient photocatalytic activity. *Journal of Environmental Chemical Engineering*, 5(6): 5521−5527.

[17] Liu, T., Dai, Y., Chen, X. (2015). Hydrothermal synthesis of CMSs@$Ag_3PO_4$ core-shell composite with enhanced photocatalytic activity. *Materials Letters*, 161: 678−681.

[18] Zheng, C., Yang, H., Yang, Y. (2017). Pseudocapacitive behavior of $Ag_3PO_4$ nanospheres prepared by a sonochemical process. *Materials Transactions*, 58(2): 298−301.

[19] Deonikar, V.G., Reddy, K.K., Chung, W.J., Kim, H. (2019). Facile synthesis of $Ag_3PO_4$/g-$C_3N_4$ composites in various solvent systems with tuned morphologies and their efficient photocatalytic activity for multi-dye degradation. *Journal of Photochemistry and Photobiology A: Chemistry*, 368: 168−181.

[20] Mohamed, S.K., Hamdy, M.S. (2019). Facile synthesis, characterization and photocatalytic activity of $Ag_3PO_4$/$Ag_2W_2O_7$ heterojunction composite. *Materials Research Express*, 6(5): 055904.

[21] Mu, C., Zhang, Y., Cui, W., Liang, Y., Zhu, Y. (2017). Removal of bisphenol A over a separation free 3D $Ag_3PO_4$-graphene hydrogel via an adsorption-photocatalysis synergy. *Applied Catalysis B: Environmental*, 212: 41–49.

[22] Zwara, J., Grabowska, E., Klimczuk, T., Lisowski, W., Zaleska-Medynska, A. (2018). Shape-dependent enhanced photocatalytic effect under visible light of $Ag_3PO_4$ particles. *Journal of Photochemistry and Photobiology A: Chemistry*, 367: 240-252.

[23] Martin, D.J., Umezawa, N., Chen, X., Ye, J., Tang, J. (2013). Facet engineered $Ag_3PO_4$ for efficient water photooxdation. *Energy & Environmental Science*, 6: 3380–3386.

[24] Ge, M. (2014). Photodegradation of Rhodamine B and methyl orange by $Ag_3PO_4$ catalyst under visible light irradiation. *Chinese Journal of Catalysis*, 35(8): 1410−1417.

[25] Guo, X., Chen, C., Yin, S., Huang, L., Qin, W. (2014). Controlled synthesis and photocatalytic properties of $Ag_3PO_4$ microcrystals. *Journal of Alloys and Compounds*, 619: 293−297.

[26] Dong, P., Yin, Y., Xu, N., Guan, R., Hou, G., Wang, Y. (2014). Facile synthesis of tetrahedral $Ag_3PO_4$ mesocrystals and its enhanced photocatalytic activity. *Materials Research Bulletin*, 60: 682–689.

[27] Sulaeman, U., Suhendar, S., Diastuti, H., Riapanitra, A., Yin, S. (2018). Design of Ag3PO4 for highly enhanced photocatalyst using hydroxyapatite as a source of phosphate ion. *Solid State Sciences*, 86: 1-5.

[28] Dong, L., Wang, P., Wang, S., Lei, P., Wang, Y. (2014). A simple way for $Ag_3PO_4$ tetrahedron and tetrapod microcrystals with high visible-light-responsive activity. *Materials Letters*, 134: 158−161.

[29] Liu, J.K., Luo, C.X., Wang, J.D., Yang, X.H., Zhong, X.H. (2012). Controlled synthesis of silver phosphate crystals with high photocatalytic activity and bacteriostatic activity. *CrystEngComm*, 14: 8714−8721.

[30] Chen, Z., Weilin, W., Zhengguo, Z., Xiaoming, F. (2013). High efficiency visible-light-driven $Ag_3PO_4$/AgI photocatalysts: Z-Scheme photocatalytic mechanism for their enhanced photocatalytic activity. *The Journal of Physical Chemistry*, 117: 19346−19352.

[31] Chong, R., Cheng, X., Wang, B., Li, D., Chang, Z., Zhang, L. (2016). Enhanced photocatalytic activity of $Ag_3PO_4$ for oxygen evolution and Methylene blue degeneration: Effect of calcination temperature. *International Journal of Hydrogen Energy*, 41(4): 2575-2582.

[32] Sadowski, J, Domagala, J.Z. (2004). Influence of defects on the lattice constant of GaMnAs. *Physical Review B*, 69(7): 7-15.

[33] Gao, Y., Masuda, Y., Koumoto, K. (2003). Band gap energy of $SrTiO_3$ thin film prepared by the liquid phase deposition method. *Journal of the Korean Ceramic Society*, 40(3): 213−218.

[34] Sulaeman, U., Nisa, I.R., Riapanitra, A., Iswanto, P., Yin, S., Sato, T. (2014). The highly active photocatalyst of silver orthophosphate under visible light irradiation for phenol oxidation. *Advanced Materials Research*, 896: 141−144.

[35] Wang, Z., Yin, L., Zhang, M., Zhaou, G., Fei, H., Shi, H., Dai, H. (2013). Synthesis and characterization of $Ag_3PO_4$/multiwalled carbon nanotube composite photocatalyst with enhanced photocatalytic activity and stability visible light. *Material Science*, 49: 1585−1593.

[36] Khan, A., Qamart, M., Muneer, M. (2012). Synthesis of highly active visible-light-driven colloidal silver orthophosphate. *Chemistry Physic Letter*, 519−520: 54−58.

[37] Hu, H., Jiao, Z., Yu, H., Lu, G., Ye, J., Bi, Y. (2013). Facile synthesis of tetrahedral $Ag_3PO_4$ submicro-crystals with enhanced photocatalytic properties. *Journal of Materials Chemistry A*, 1: 2387–2390.

[38] Yang, Y., Guo, Y., Hu, C., Jiang, C., Wang, E. (2003). Synergistic effect of Keggin-type $[X^{n+}W_{11}O_{39}]^{(12-n)-}$ and $TiO_2$ in macroporous hybrid materials $[X^{n+}W_{11}O_{39}]^{(12-n)-}$–$TiO_2$ for the photocatalytic degradation of textile dyes. *Journal of Materials Chemistry*, 13: 1686–1694.

[39] Grilla, E., Petala, A., Frontistis, Z., Konstantinou, I.K., Kondarides, D.I., Mantzavinos, D. (2018). Solar photocatalytic abatement of sulfamethoxazole over $Ag_3PO_4$/$WO_3$ composites. Applied Catalysis B: Environmental, 231: 73–81.